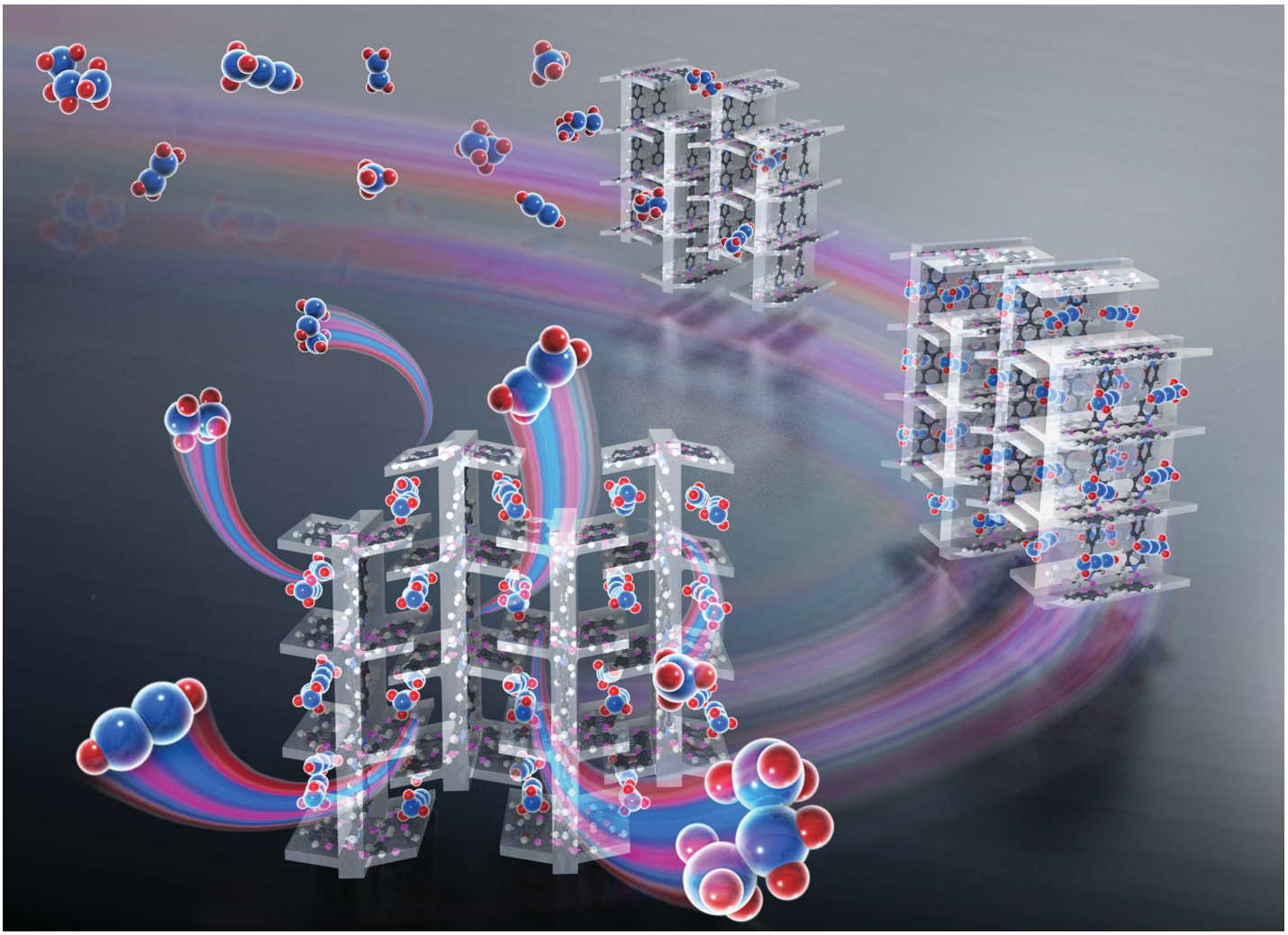

Showcasing the study on C1/C2/C3 hydrocarbons separation of flexible MOFs by Dr. Libo Li and Prof. Jinping Li at Research Institute of Special Chemicals, Taiyuan University of Technology and Prof. Rajamani Krishna at Van 't Hoff Institute for Molecular Sciences, University of Amsterdam.

Title: Exploiting the gate opening effect in a flexible MOF for selective adsorption of propyne from C1/C2/C3 hydrocarbons

A flexible MOF [Cu(dhbc)$_2$(4,4'-bipy)], with gate-opening characteristics, exhibits adsorption selectivity in favor of propyne in a C1/C2/C3 mixture of hydrocarbons. A combination of measurements of unary isotherms, IAST calculations, and breakthrough experiments and simulations showed that propyne can be selectively adsorbed from C1/C2/C3 hydrocarbons in fixed bed adsorbers that are commonly employed in process industries.

As featured in:

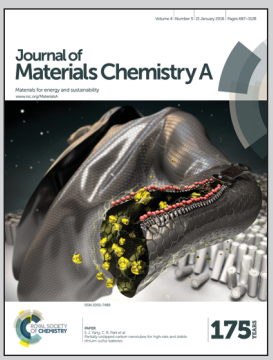

See Jiangfeng Yang, Jinping Li *et al.*, *J. Mater. Chem. A*, 2016, **4**, 751.

ROYAL SOCIETY OF CHEMISTRY

www.rsc.org/MaterialsA

Registered charity number: 207890

Journal of Materials Chemistry A

COMMUNICATION

View Article Online
View Journal | View Issue

Cite this: J. Mater. Chem. A, 2016, 4, 751

Received 9th November 2015
Accepted 25th November 2015

DOI: 10.1039/c5ta09029f

www.rsc.org/MaterialsA

Exploiting the gate opening effect in a flexible MOF for selective adsorption of propyne from C1/C2/C3 hydrocarbons†

Libo Li,[a] Rajamani Krishna,[b] Yong Wang,[a] Jiangfeng Yang,*[a] Xiaoqing Wang[a] and Jinping Li*[a]

The separation of propyne from light hydrocarbon mixtures is of technological importance but poses considerable technical challenges. This article reports on the potential of a flexible metal–organic framework [Cu(dhbc)$_2$(4,4′-bipy)], with gate-opening characteristics, that exhibits adsorption selectivity in favor of propyne in a C1/C2/C3 mixture of hydrocarbons. The separation potential of the flexible MOF is established using a judicious combination of measurements of unary isotherms, IAST calculations of mixture adsorption equilibrium, transient breakthrough simulations, along with transient breakthrough experiments. Our multi-tier investigation strategy confirms that propyne can be selectively adsorbed from C1/C2/C3 hydrocarbons in fixed bed adsorbers that are commonly employed in the process industries.

Light hydrocarbons such as C_2H_4, and C_3H_6 are important feedstock in petrochemical industries for the production of polyethylene and polypropylene. The separation and isolation of such feedstock from hydrocarbon mixtures is traditionally carried out in distillation columns that are energy demanding. Adsorptive separation is an alternative method to cryogenic distillation and is more sustainable. Initially, some zeolites were considered adsorbents for light hydrocarbon separation; Miltenburg tested the separation of ethane/ethylene mixtures by working with CuCl/NaX;[1a] Rodrigues reported the use of zeolite 13X for separation of propane/propylene mixtures;[1b] Al-Baghli suggested that Na-ETS-10 have great potential as adsorbents for ethylene/ethane separations.[1c] However, these zeolites have an average kinetic diameter of 8–10 Å, which is larger than the molecular diameter of light hydrocarbons; so the separation selectivity on zeolites would be based on equilibrium competitive adsorption.[1d] In recent years, there has been considerable research on the synthesis of metal–organic frameworks (MOFs) that offer energy-efficient alternatives to distillation technology.[2] The potential of MOFs has been well established for a variety of separations: C_2H_2/C_2H_4,[2d,3] C_2H_4/C_2H_6,[2d,3a,4] C_3H_6/C_3H_8,[2d,3a,5a] $CH_4/C_2H_2/C_2H_4/C_2H_6$,[3a,5b,c] and $CH_4/C_2H_2/C_2H_4/C_2H_6/C_3H_6/C_3H_8$ mixtures.[3a,5d] The feedstock for polymerization reactors needs to be free of impurities such as C_2H_2 (acetylene = ethyne) and C_3H_4 (methyl acetylene = propyne) that have a tendency to poison the catalysts. While there has been considerable published research on C_2H_2/C_2H_4 separations, there is no published work on selective adsorption of C_3H_4. In this work, we present the first example where separations of C_3H_4 from $CH_4/C_2H_2/C_2H_4/C_2H_6/C_3H_6/C_3H_8$ mixtures are achieved with a single flexible MOF [Cu(dhbc)$_2$(4,4′-bipy)] utilizing guest-induced structural changes and the resulting differences in gate-opening pressures.

Flexible MOFs as promising materials for gas separation have attracted a lot of attention, but such expectations have commonly been based solely on inspection of their pure-component adsorption isotherms. The efficacy of flexible MIL-53 for a variety of separations is published in a number of publications.[6]

The flexible MOF [Cu(dhbc)$_2$(4,4′-bipy)] exhibits unique gate-opening behavior at certain pressures of nitrogen, oxygen, or methane, corresponding to a subnetwork displacement in its structure; this was first reported by Kitagawa in 2003.[7] As a consequence of such structural changes, [Cu(dhbc)$_2$(4,4′-bipy)] exhibits adsorption selectivity between two kinds of guest molecules that exploits the differences in the gate opening pressures. In recent work, carried out using an in-house-constructed separation apparatus, controlled and targeted CO_2 and CH_4 capture, respectively, from binary mixtures (CO_2/CH_4 or CH_4/N_2) has been realized with [Cu(dhbc)$_2$(4,4′-bipy)].[8]

[a]College of Chemistry and Chemical Engineering, Taiyuan University of Technology, Taiyuan 030024, Shanxi, P. R. China. E-mail: jpli211@hotmail.com; yangjiangfeng@tyut.edu.cn

[b]Van 't Hoff Institute for Molecular Sciences, University of Amsterdam, Science Park 904, 1098 XH Amsterdam, The Netherlands

† Electronic supplementary information (ESI) available: Experimental details, fitting of experimental data on pure component isotherms, GCMC simulation details, breakthrough curves for equimolar 3-component $C_2H_6/C_2H_4/C_2H_2$ and CH_4–C_2H_6–C_3H_8 mixtures and equimolar 2-component C_2H_4/C_3H_6 mixtures, and video animations of the transient traversal of gas phase concentrations along the length of the fixed bed adsorber. See DOI: 10.1039/c5ta09029f

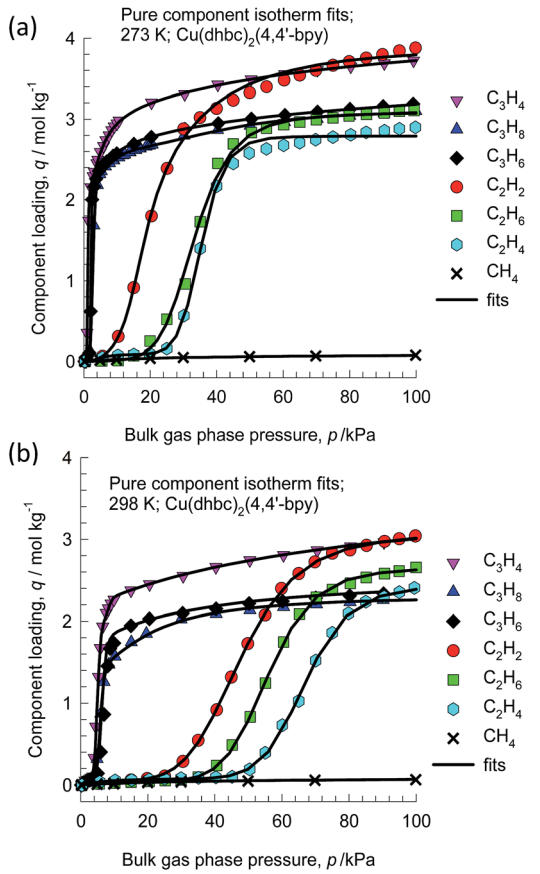

Fig. 1 Comparisons of experimental data for unary isotherms for CH_4, C_2H_2, C_2H_4, and C_2H_6, C_3H_4, C_3H_6, and C_3H_8 at (a) 273 K and (b) 298 K in [Cu(dhbc)$_2$(4,4′-bipy)] with multi-site Langmuir–Freundlich model fits.

In this article, we investigated the potential of [Cu(dhbc)$_2$(4,4′-bipy)] for light hydrocarbon separations. Unary isotherms for C1–C3 hydrocarbon adsorption were measured on [Cu(dhbc)$_2$(4,4′-bipy)] at 273 and 298 K. Fig. 1 presents comparisons of experimental data for unary isotherms for CH_4, C_2H_2, C_2H_4, and C_2H_6, C_3H_4, C_3H_6, and C_3H_8 in [Cu(dhbc)$_2$(4,4′-bipy)] at (a) 273 K and (b) 298 K with multi-site Langmuir–Freundlich model fits; the fit parameters are provided in the ESI† accompanying this article. The fits are of good accuracy at both temperatures.

The unary isotherm of each C2–C3 hydrocarbon displays gate opening characteristics (Fig. 1). The structural transformation in flexible MOFs was due to the guest-induced phenomenon; the stronger intermolecular interactions between guest molecules and flexible MOFs led to a lower gate-opening pressure. So at lower temperatures, thermal motion of gases would be lower, so that the gas molecules can get adsorbed on the flexible MOFs easily, thereby causing a lower gate-opening pressure.[8–10] And as a common sense in flexible MOFs, the interaction energy between MOF structures and guest molecules is dependent on the gate-opening phenomenon. The results showed that the interaction energy is larger for C3 hydrocarbon *vs.* C2 hydrocarbon molecules. Therefore, the longer the chain of the guest hydrocarbon, the more likely the flexible MOF structures are affected by this interaction and the lower is the pressure opening point, as shown in Fig. 1.[2a] And C_3H_4 has the lowest gate-opening pressure to induce the structural transitions of the flexible MOF [Cu(dhbc)$_2$(4,4′-bipy)], which indicated that the flexible framework can highly selectively adsorb C_3H_4 at a very low pressure. Interestingly, there is a discernible trend in the gate-opening pressures of guest molecules in [Cu(dhbc)$_2$(4,4′-bipy)], as outlined below.

The gate-opening pressures of C2–C3 hydrocarbons on [Cu(dhbc)$_2$(4,4′-bipy)] at 273 and 298 K are found to inversely correlate very well with the latent heat of vaporization, whose values are, respectively, 16.6, 12.5, 13.9, 20.9, 17.7, and 19.1 kJ mol^{-1}; see Fig. 2. And the molar enthalpy of gate opening correlates with the molar enthalpy of vaporization, see Fig. S2.† Thus, we speculate that a condensation phenomenon occurs during adsorption of light hydrocarbons in the flexible MOF, triggering the gate-opening process. A similar phenomenon was reported by Yaghi on rigid MOFs.[11] Yaghi *et al.* have explained the unusual shape of adsorption isotherms in IRMOF-1, through combining with GCMC simulations and experiment results. They explained that the attractive electrostatic interactions between gas molecules were responsible for the unusual shape of the adsorption isotherms, and the pore was filled with the guest molecules in the condensed phase.

The simulation results are presented in Fig. 3 as snapshots of the locations and conformations of C_2H_6 and C_2H_4 adsorbed within the channels of the structure.[14] It is noticed that, in the one-dimensional channel, C_2H_6 and C_2H_4 align along the center of the channels. These snapshots also validate the hypothesis that light hydrocarbons adsorb in [Cu(dhbc)$_2$(4,4′-bipy)] following a condensation process. The reason may be attributed to the fact that suitable pore sizes fixed the hydrocarbon molecule isolate in the one-dimensional channel. To further study the mechanism of gas diffusion through the one-dimensional pores of [Cu(dhbc)$_2$(4,4′-bipy)], a new model was designed for MD (molecular dynamics) simulations. And the results showed that light hydrocarbon molecules can easily diffuse through the one-dimensional channels, and no pore size

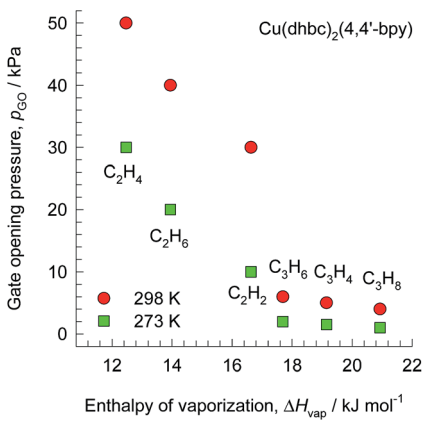

Fig. 2 The gate opening pressures of C_2H_2, C_2H_4, C_2H_6, C_3H_4, C_3H_6, and C_3H_8 at 273 K and 298 K in [Cu(dhbc)$_2$(4,4′-bipy)] plotted as a function of latent heats of vaporization.

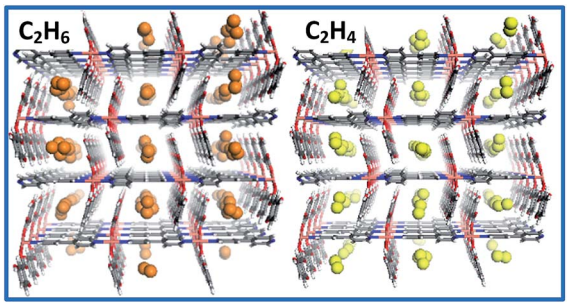

Fig. 3 A schematic from a GCMC simulation for C_2H_6 (brown), and C_2H_4 (yellow) adsorption in the channels of [Cu(dhbc)$_2$(4,4′-bipy)] at 1 bar and 273 K.[12,13]

limitation to diffusion was found (Fig. S4†). A similar behavior was reported by Kitagawa *et al.*, who showed that C_2H_2 adsorbed in the channels of $Cu_2(pzdc)_2(pyz)$ (pzdc = pyrazine-2,3-dicarboxylate and pyz = pyrazine) through the electrostatic attraction and electron delocalization effect between the hydrogen atom of C_2H_2 and the free oxygen atom.[15]

The strength of C1–C3 hydrocarbons binding within [Cu(dhbc)$_2$(4,4′-bipy)] was determined quantitatively through analysis of the gas adsorption data. The binding energy of the adsorbate that is reflected in the isosteric heat of adsorption, Q_{st}, was determined using the pure component isotherm fits using the Clausius–Clapeyron equation (Fig. S3†). The results showed that C_3H_4 has the highest binding energy in C1–C3 hydrocarbons, which implies that [Cu(dhbc)$_2$(4,4′-bipy)] can selectively adsorb C_3H_4 from hydrocarbon mixtures.

Furthermore, the ideal adsorbed solution theory (IAST) was calculated to estimate the adsorption of equimolar 7-component $CH_4/C_2H_2/C_2H_4/C_2H_6/C_3H_4/C_3H_6/C_3H_8$ gas mixtures (Fig. 4), and adsorption selectivities of C_3H_4/C_3H_6, C_3H_6/C_3H_8, C_3H_6/C_2H_4, and C_2H_4/CH_4 in [Cu(dhbc)$_2$(4,4′-bipy)] (Fig. 5). The component loadings were bunched into three fractions: C3, C2 and C1 hydrocarbons with different carbon numbers. The longer the chain of the guest hydrocarbon, the stronger is the binding energy between MOF structures. And at both temperatures C_3H_4 has the highest component loading in [Cu(dhbc)$_2$(4,4′-bipy)], which indicates that C_3H_4 can be selectively adsorbed from hydrocarbon mixtures. For adsorption of equimolar 7-component $CH_4/C_2H_2/C_2H_4/C_2H_6/C_3H_4/C_3H_6/C_3H_8$ gas mixtures, the calculated C_2H_4/CH_4 selectivities are 1000, and this value is much higher than the recently reported values (300 for $Fe_2(dobdc)$).[2d]

To confirm the selective adsorption of C_3H_4 over C_3H_6 and C_3H_8 under mixture conditions, several breakthrough experiments were performed on an in-house-constructed apparatus, which was reported in our previous work (Fig. S5†).[8,16] The breakthrough experiments were performed to demonstrate the selective adsorption of C_3H_4 using [Cu(dhbc)$_2$(4,4′-bipy)], in which equimolar 3-component $C_3H_4/C_3H_6/C_3H_8$ mixtures were flowed over a packed bed with a total flow rate of 30 mL min^{-1} at 298 K. As shown in Fig. 6a, with the high adsorption selectivity of [Cu(dhbc)$_2$(4,4′-bipy)], C_3H_6 and C_3H_8 break first, while C_3H_4 breaks through after some period of time. And C_3H_4 can be

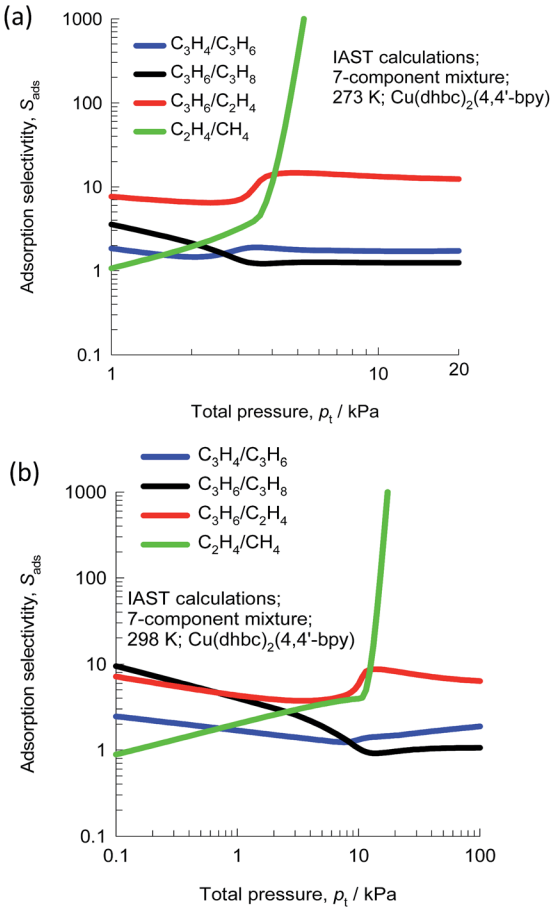

Fig. 4 IAST calculations for component loadings for adsorption of 7-component $CH_4/C_2H_2/C_2H_4/C_2H_6/C_3H_4/C_3H_6/C_3H_8$ gas mixtures in [Cu(dhbc)$_2$(4,4′-bipy)] at (a) 273 K and (b) 298 K.

effectively separated from the $C_3H_4/C_3H_6/C_3H_8$ mixtures in a nearly pure form with the gas phase concentrations of more than 99.9% (detection limit ~ 0.1%). And the breakthrough experiment results are in agreement with the expectations of the IAST calculations of mixture adsorption shown in Fig. 4 and 5.

The experimental breakthroughs for $C_3H_4/C_3H_6/C_3H_8$ mixtures are in very good agreement with transient breakthrough simulations (Fig. 6b) carried out using the methodology described in previous work.[2f] In both experiments and simulations, we note that C_3H_4 is the last component to elute from the fixed bed confirming that this component can be selectively adsorbed from the C3 hydrocarbons.

The breakthrough experiments were also performed on equimolar 3-component $C_2H_6/C_2H_4/C_2H_2$ and CH_4–C_2H_6–C_3H_8 mixtures and equimolar 2-component C_2H_4/C_3H_6 mixtures; see Fig. S6–S8 of the ESI† accompanying this article. These breakthrough experiments confirm the adsorption hierarchy observed in Fig. 4: $CH_4 < C_2H_4 < C_2H_6 < C_3H_6 < C_3H_8 < C_3H_4$. By combination with the IAST calculations and breakthrough experiments, we can conclude that the flexible MOF [Cu(dhbc)$_2$(4,4′-bipy)] can selectively adsorb C_3H_4 from C1–C3 hydrocarbon mixtures with its unique gate-opening phenomenon.

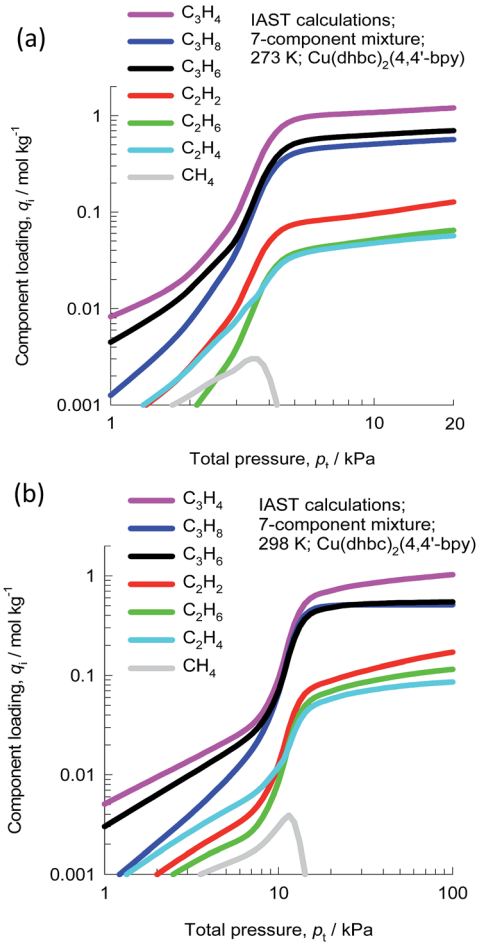

Fig. 5 IAST calculations for C_3H_4/C_3H_6, C_3H_6/C_3H_8, C_3H_6/C_2H_4, and C_2H_4/CH_4 adsorption selectivities for 7-component $CH_4/C_2H_2/C_2H_4/C_2H_6/C_3H_4/C_3H_6/C_3H_8$ gas mixture adsorption in [Cu(dhbc)$_2$(4,4′-bipy)] maintained under isothermal conditions at (a) 273 K and (b) 298 K.

To further confirm this conclusion, we carried out transient breakthrough simulations with a 7-component $CH_4/C_2H_2/C_2H_4/C_2H_6/C_3H_4/C_3H_6/C_3H_8$ fed to a fixed bed adsorber operating at 298 K; see Fig. 7. The sequence of breakthroughs is CH_4, C_2H_6, C_2H_4, C_2H_2, C_3H_8, C_3H_6, and C_3H_4. This sequence indicates that C_3H_4 can also be selectively adsorbed from a C1/C2/C3 mixture. As C1–C2 hydrocarbons cannot get adsorbed on [Cu(dhbc)$_2$(4,4′-bipy)] at that pressure, they were diffused through the fixed bed at the very beginning, which is because this pressure is lower than their gate-opening pressure. Particularly noteworthy is the long time interval between the breakthroughs of C2 and C3 hydrocarbons, which showed that flexibility is being used to effect a more efficient separation. This is a direct consequence of the large differences in the gate-opening pressures of C3 hydrocarbons compared to C2 hydrocarbons as witnessed in Fig. 7. The separation potential of [Cu(dhbc)$_2$(4,4′-bipy)] is best appreciated by video animations of the transient traversal of gas phase concentrations along the length of the fixed bed adsorber; this video has been uploaded as ESI† in this publication.

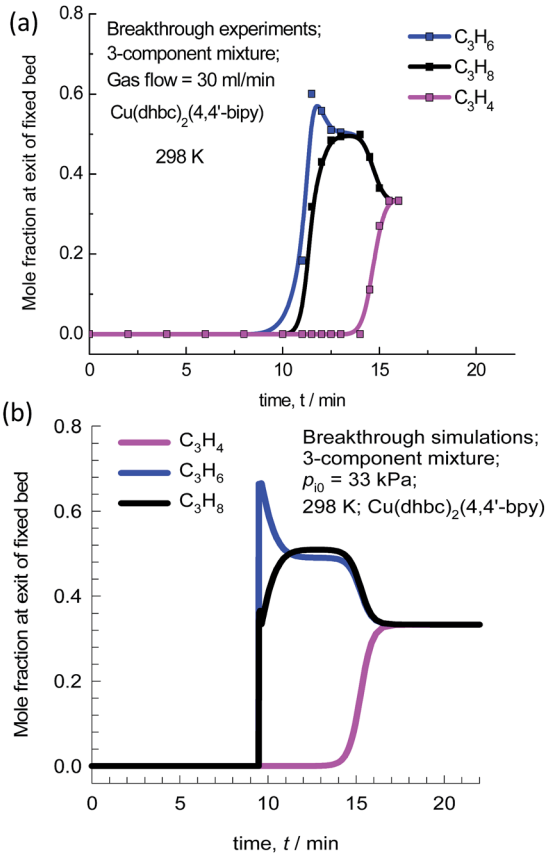

Fig. 6 Breakthrough experiments (a) and simulations (b) of [Cu(dhbc)$_2$(4,4′-bipy)] for separation of equimolar 3-component C_3H_4–C_3H_6–C_3H_8 mixtures in a fixed bed of adsorbent at 298 K.

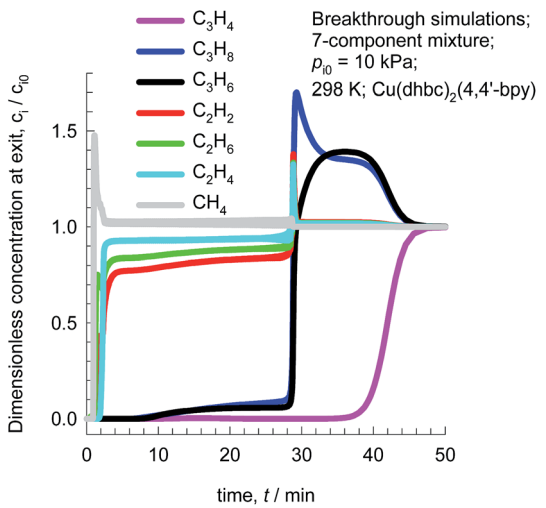

Fig. 7 Breakthrough simulation with an equimolar 7-component $CH_4/C_2H_2/C_2H_4/C_2H_6/C_3H_4/C_3H_6/C_3H_8$ mixture into a fixed bed of adsorbent. The inlet partial pressures are 10 kPa for each hydrocarbon.

Conclusions

In summary, the flexible MOF [Cu(dhbc)$_2$(4,4′-bipy)] with unique gate-opening behavior has been studied for separation

of C_3H_4 from C1–C3 hydrocarbon mixtures. The separation potential of the flexible MOF is established by a combination of measurements of unary isotherms, IAST calculations of mixture adsorption equilibrium, transient breakthrough simulations, along with transient breakthrough experiments. The results exhibited that [Cu(dhbc)$_2$(4,4′-bipy)] is promising for selective adsorption of C_3H_4 from C1–C3 hydrocarbon mixtures.

Acknowledgements

We gratefully acknowledge the financial support from the National Natural Science Foundation of China (No. 21136007, 51302184) and the National Research Fund for Fundamental Key Projects (No. 2014CB260402). We thankfully acknowledge Prof. Chongli Zhong (Beijing University of Chemical Technology) for providing their in-house code CADSS (Complex Adsorption and Diffusion Simulation Suite) in Grand canonical Monte Carlo (GCMC) simulations.

Notes and references

1 (*a*) A. V. Miltenburg, J. Gascon, W. Zhu, F. Kapteijn and J. A. Moulijn, *Adsorption*, 2008, **14**, 309; (*b*) P. S. Gomes, N. Lamia and A. E. Rodrigues, *Chem. Eng. Sci.*, 2009, **64**, 1336; (*c*) N. A. Al-Baghli and K. F. Loughlin, *J. Chem. Eng. Data*, 2006, **51**, 248; (*d*) M. Shi, A. M. Avila, F. Yang, T. M. Kuznicki and S. M. Kuznicki, *Chem. Eng. Sci.*, 2011, **66**, 2817.

2 (*a*) N. Nijem, H. Wu, P. Canepa, A. Marti, K. J. Balkus Jr, T. Thonhauser, J. Li and Y. J. Chabal, *J. Am. Chem. Soc.*, 2012, **134**, 15201; (*b*) D. Peralta, G. Chaplais, A. Simon-Masseron, K. Barthelet, C. Chizallet, A.-A. Quoineaud and G. D. Pirngruber, *J. Am. Chem. Soc.*, 2012, **134**, 8115; (*c*) Y. Bae, C. Y. Lee, K. C. Kim, O. K. Farha, P. Nickias, J. T. Hupp, S. T. Nguyen and R. Q. Snurr, *Angew. Chem., Int. Ed.*, 2012, **51**, 1857; (*d*) E. D. Bloch, W. L. Queen, R. Krishna, J. M. Zadrozny, C. M. Brown and J. R. Long, *Science*, 2012, **335**, 1606; (*e*) Y. He, W. Zhou, R. Krishna and B. Chen, *Chem. Commun.*, 2012, **48**, 11813; (*f*) R. Krishna, *RSC Adv.*, 2015, **5**, 52269; (*g*) R. Krishna, *Phys. Chem. Chem. Phys.*, 2015, **17**, 39.

3 (*a*) Y. He, R. Krishna and B. Chen, *Energy Environ. Sci.*, 2012, **5**, 9107; (*b*) T. L. Hu, H. Wang, B. Li, R. Krishna, H. Wu, W. Zhou, Y. Zhao, Y. Han, X. Wang, W. Zhu, Z. Yao, S. C. Xiang and B. Chen, *Nat. Commun.*, 2015, **6**, 7328; (*c*) M. C. Das, Q. Guo, Y. He, J. Kim, C. G. Zhao, K. Hong, S. Xiang, Z. Zhang, K. M. Thomas, R. Krishna and B. Chen, *J. Am. Chem. Soc.*, 2012, **134**, 8703; (*d*) H. M. Wen, B. Li, H. Wang, C. Wu, K. Alfooty, R. Krishna and B. Chen, *Chem. Commun.*, 2015, **51**, 5610.

4 (*a*) S. Yang, A. J. Ramirez-Cuesta, R. Newby, V. Garcia-Sakai, P. Manuel, S. K. Callear, S. I. Campbell, C. C. Tang and M. Schröder, *Nat. Chem.*, 2014, **7**, 121; (*b*) B. Li, Y. Zhang, R. Krishna, K. Yao, Y. Han, Z. Wu, D. Ma, Z. Shi, T. Pham, B. Space, J. Liu, P. K. Thallapally, J. Liu, M. Chrzanowski and S. Ma, *J. Am. Chem. Soc.*, 2014, **136**, 8654; (*c*) Y. Zhang, B. Li, R. Krishna, Z. Wu, D. Ma, Z. Shi, T. Pham, K. Forrest, B. Space and S. Ma, *Chem. Commun.*, 2015, **51**, 2714; (*d*) D. L. Chen, N. Wang, C. Xu, G. Tu, W. Zhu and R. Krishna, *Microporous Mesoporous Mater.*, 2015, **208**, 55; (*e*) P. Li, Y. He, H. D. Arman, R. Krishna, L. Weng and B. Chen, *Chem. Commun.*, 2014, **50**, 13081.

5 (*a*) D. L. Chen, H. Shang, W. Zhu and R. Krishna, *Chem. Eng. Sci.*, 2014, **117**, 407; (*b*) J. Duan, W. Jin and R. Krishna, *Inorg. Chem.*, 2015, **54**, 4279; (*c*) Y. He, C. Song, Y. Ling, C. Wu, R. Krishna and B. Chen, *APL Mater.*, 2014, **2**, 124102; (*d*) J. Jia, L. Wang, F. Sun, X. Jing, Z. Bian, K. Cai, L. Gao, R. Krishna and G. S. Zhu, *Chem.–Eur. J.*, 2014, **20**, 9073.

6 (*a*) T. Rodenas, M. van Dalen, E. García-Pérez, P. Serra-Crespo, B. Zornoza, F. Kapteijn and J. Gascon, *Adv. Funct. Mater.*, 2014, **24**, 249; (*b*) N. Rosenbach Jr, A. Ghoufi, I. Déroche, P. L. Llewellyn, T. Devic, S. Bourrelly, C. Serre, G. Férey and G. Maurin, *Phys. Chem. Chem. Phys.*, 2010, **12**, 6428; (*c*) P. L. Llewellyn, P. Horcajada, G. Maurin, T. Devic, N. Rosenbach, S. Bourrelly, C. Serre, D. Vincent, S. Loera-Serna, Y. Filinchuk and G. Férey, *J. Am. Chem. Soc.*, 2009, **131**, 13002; (*d*) T. K. Trung, P. Trens, N. Tanchoux, S. Bourrelly, P. L. Llewellyn, S. Loera-Serna, C. Serre, T. Loiseau, F. Fajula and G. Férey, *J. Am. Chem. Soc.*, 2008, **130**, 16926.

7 R. Kitaura, K. Seki, G. Akiyama and S. Kitagawa, *Angew. Chem., Int. Ed.*, 2003, **42**, 428.

8 L. Li, Y. Wang, J. Yang, X. Wang and J. Li, *J. Mater. Chem. A*, 2015, **3**, 22574.

9 L. Li, J. Yang, Q. Zhao and J. Li, *CrystEngComm*, 2013, **15**, 1689.

10 J. Lin, J. Zhang, W. Zhang, W. Xue, D. Xue and X. Chen, *Inorg. Chem.*, 2009, **48**, 6652.

11 K. S. Walton, A. R. Millward, D. Dubbeldam, H. Frost, J. J. Low, O. M. Yaghi and R. Q. Snurr, *J. Am. Chem. Soc.*, 2008, **130**, 406.

12 M. Tong, Q. Yang, Y. Xiao and C. Zhong, *Phys. Chem. Chem. Phys.*, 2014, **16**, 15189.

13 (*a*) Q. Xu and C. Zhong, *J. Phys. Chem. C*, 2010, **114**, 5035; (*b*) C. Zheng and C. Zhong, *J. Phys. Chem. C*, 2010, **114**, 9945.

14 Z. R. Herm, B. M. Wiers, J. A. Mason, J. M. Baten, M. R. Hudson, P. Zajdel, C. M. Brown, N. Masciocchi, R. Krishna and J. R. Long, *Science*, 2013, **340**, 960.

15 R. Matsuda, R. Kitaura, S. Kitagawa, Y. Kubota, R. V. Belosludov, T. C. Kobayashi, H. Sakamoto, T. Chiba, M. Takata, Y. Kawazoe and Y. Mita, *Nature*, 2005, **436**, 238.

16 L. Li, J. Yang, J. Li, Y. Chen and J. Li, *Microporous Mesoporous Mater.*, 2014, **198**, 236.

Exploiting the Gate Opening Effect in a Flexible MOF for Selective Adsorption of Propyne from C1/C2/C3 Hydrocarbons

Libo Li,[a] Rajamani Krishna,[b] Yong Wang,[a] Jiangfeng Yang,[a,*] and Jinping Li [a,*]

[a]College of Chemistry and Chemical Engineering, Taiyuan University of Technology, Taiyuan 030024, Shanxi, P. R. China. Email: jpli211@hotmail.com

[b]Van 't Hoff Institute for Molecular Sciences, University of Amsterdam, Science Park 904, 1098 XH Amsterdam, The Netherlands.

Contents

1. Synthesis of [Cu(dhbc)$_2$(4,4'-bipy)]

Syntheses of [Cu(dhbc)$_2$(4,4'-bipy)]·H_2O were first reported by S. Kitagawa in 2003, and the synthetic processes were subsequently improved as described in our previous work. All chemicals were purchased in their highest available commercial purity (>98%) from Sigma–Aldrich.

[Cu(dhbc)$_2$(4,4'-bipy)]·H_2O: an ethanol solution (10 mL) containing a mixture of 4,4'-bipyridine (0.125 g, 0.8 mmol) and 2,5-dihydroxybenzoic acid (0. 49 g, 3.2 mmol) was carefully layered on

the top of an aqueous solution (10 mL) of $Cu(NO_3)_2 \cdot 3H_2O$ (0.099 g, 0.4 mmol), after which green crystals began to form immediately. Three days later, the green crystals were collected by filtration, and were then washed with ethanol (Yield > 80%).

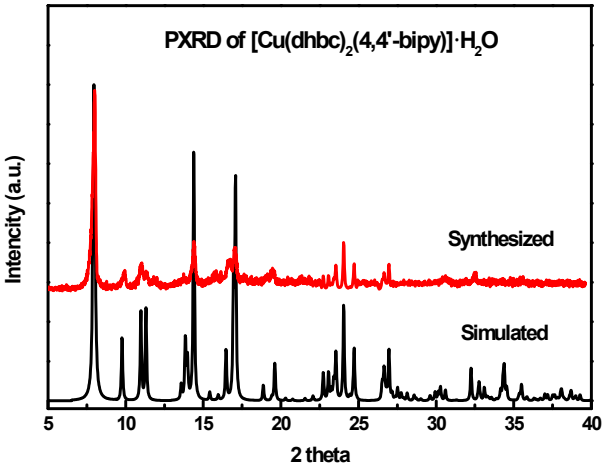

Figure S1. PXRD data for as-synthesized $[Cu(dhbc)_2(4,4'\text{-bipy})]\cdot H_2O$.

2. Fitting of experimental data on pure component isotherms

The isotherm data for CH_4 were fitted with the single-site Langmuir-Freundlich model

$$q = q_{sat}\frac{bp^{v}}{1 + b_A p^{v}} \tag{1}$$

with T-dependent parameter

$$b = b_0 exp(\frac{E}{RT}) \tag{2}$$

The isotherm data for C_2H_2, C_2H_4, and C_2H_6 were fitted with the Dual-site Langmuir-Freundlich model, individually for each temperature

$$q = q_{A,sat}\frac{b_A p^{v_A}}{1 + b_A p^{v_A}} + q_{B,sat}\frac{b_B p^{v_B}}{1 + b_B p^{v_B}} \tag{3}$$

The pure component isotherm data for C_3H_4, C_3H_6 and C_3H_8 display multiple inflections and a proper description of these is provided by the 3-site Langmuir-Freundlich model:

$$q = q_{A,sat}\frac{b_A p^{v_A}}{1 + b_A p^{v_A}} + q_{B,sat}\frac{b_B p^{v_B}}{1 + b_B p^{v_B}} + q_{C,sat}\frac{b_C p^{v_C}}{1 + b_C p^{v_C}} \tag{4}$$

The saturation capacities q_{sat}, Langmuir constants b, and the Freundlich exponents ν, for CH_4, C_2H_2, C_2H_4, and C_2H_6, C_3H_4, C_3H_6 and C_3H_8 are provided in supporting information.

The 1-site Langmuir-Freundlich model parameters for CH_4 are specified in Table 1. And the 2-site Langmuir-Freundlich parameters for C_2H_2, C_2H_4, and C_2H_6 are provided in Table 2, and Table 3. And the saturation capacities q_{sat}, Langmuir constants b, and the Freundlich exponents ν, for C_3H_4, C_3H_6 and C_3H_8 are provided in Table 4, and Table 5.

Table 1 T-dependent Langmuir-Freundlich parameter fits for CH_4 in [Cu(dhbc)$_2$(4,4'-bipy)].

	q_{sat} (mol kg^{-1})	**b_0 (Pa^{-1})**	**ν (dimensionless)**	**E (kJ mol^{-1})**
CH_4	0.1	1.15×10^{-6}	0.95	8.5

Table 2 2-site Langmuir-Freundlich parameters for C_2H_2, C_2H_4, and C_2H_6 at 273 K in [Cu(dhbc)$_2$(4,4'-bipy)].

	Site A			**Site B**		
	$q_{i,A,sat}$ (mol kg^{-1})	$b_{i,A}$ (Pa^{-Vi})	$v_{i,A}$ (dimensionless)	$q_{i,A,sat}$ (mol kg^{-1})	$b_{i,A}$ (Pa^{-Vi})	$v_{i,A}$ (dimensionless)
C_2H_2	1.4	2.35×10^{-25}	5.8	2.5	3.58×10^{-11}	2.36
C_2H_4	2.7	3.25×10^{-46}	10	0.09	3.2×10^{-10}	2.55
C_2H_6	2.9	1.52×10^{-28}	6.15	0.2	2.43×10^{-10}	2.1

Table 3 2-site Langmuir-Freundlich parameters for C_2H_2, C_2H_4, and C_2H_6 at 298 K in [Cu(dhbc)$_2$(4,4'-bipy)].

	Site A			**Site B**		
	$q_{i,A,sat}$ (mol kg^{-1})	$b_{i,A}$ (Pa^{-Vi})	$v_{i,A}$ (dimensionless)	$q_{i,A,sat}$ (mol kg^{-1})	$b_{i,A}$ (Pa^{-Vi})	$v_{i,A}$ (dimensionless)
C_2H_2	3	2.82×10^{-26}	5.46	0.06	2.87×10^{-7}	1.7
C_2H_4	2.35	1.82×10^{-49}	10.1	0.08	3.17×10^{-6}	1.44
C_2H_6	2.6	3.49×10^{-39}	8.1	0.05	5.56×10^{-7}	1.6

Table 4 3-site Langmuir-Freundlich parameters for C_3H_4, C_3H_6 and C_3H_8 at 273 K in [Cu(dhbc)$_2$(4,4'-bipy)].

	C_3H_4	C_3H_6	C_3H_8
$q_{A,sat}$ (mol kg^{-1})	2.1	2	2.3
b_A (Pa^{-ViA})	4.2×10^{-27}	3.45×10^{-59}	7.87×10^{-27}
v_A (dimensionless)	8.55	17.5	7.6
$q_{B,sat}$ (mol kg^{-1})	0.85	0.7	0.33
b_B (Pa^{-ViB})	8.16×10^{-9}	1.04×10^{-6}	6.87×10^{-15}
v_B (dimensionless)	2.2	1.6	3.6
$q_{C,sat}$ (mol kg^{-1})	1.5	0.93	0.49
b_C (Pa^{-ViC})	4.96×10^{-5}	5.53×10^{-6}	1.1×10^{-13}
v_C (dimensionless)	0.89	1.06	2.8

Table 5 3-site Langmuir-Freundlich parameters for C_3H_4, C_3H_6 and C_3H_8 at 298 K in [Cu(dhbc)$_2$(4,4'-bipy)].

	C_3H_4	C_3H_6	C_3H_8
$q_{A,sat}$ (mol kg^{-1})	0.2	1.63	1.33
b_A (Pa^{-ViA})	9.72×10^{-72}	3.5×10^{-41}	2.95×10^{-40}
v_A (dimensionless)	18.1	10.5	10.5
$q_{B,sat}$ (mol kg^{-1})	1.8	0.94	0.98
b_B (Pa^{-ViB})	2.91×10^{-5}	1.51×10^{-5}	2.63×10^{-8}
v_B (dimensionless)	0.91	1.07	1.77
$q_{C,sat}$ (mol kg^{-1})	1.9	0.6	0.5
b_C (Pa^{-ViC})	3.38×10^{-39}	3.26×10^{-10}	3.27×10^{-10}
v_C (dimensionless)	10.4	0.64	0.65

Notation

b_A Langmuir-Freundlich constant for species i at adsorption site A, Pa^{-ViA}

b_B Langmuir-Freundlich constant for species i at adsorption site B, Pa^{-ViB}

b_C Langmuir-Freundlich constant for species i at adsorption site C, Pa^{-ViC}

E energy parameter, J mol^{-1}

p_i partial pressure of species i in mixture, Pa

p_t total system pressure, Pa

q_i component molar loading of species i, mol kg^{-1}

q_{st} isosteric heat of adsorption, J mol^{-1}

t time, s

T absolute temperature, K

Greek letters

v Freundlich exponent, dimensionless

3. Molar enthalpy of gate opening

The Clausius–Clapeyron equation can be used to calculate the molar enthalpy of gate opening, ΔH_{GO}, from the $p_{GO}(T)$ behavior of the adsorption branch of the unary isotherms of C_2H_2, C_2H_4, C_2H_6, C_3H_4, C_3H_6, and C_3H_8 at 273 K, and 298 K using

$$\Delta H_{GO} = RT^2 \left(\frac{\partial \ln p_{GO}}{\partial T} \right) \tag{5}$$

The molar enthalpy of gate opening, ΔH_{GO}, correlates with the molar enthalpy of vaporization, ΔH_{vap}.

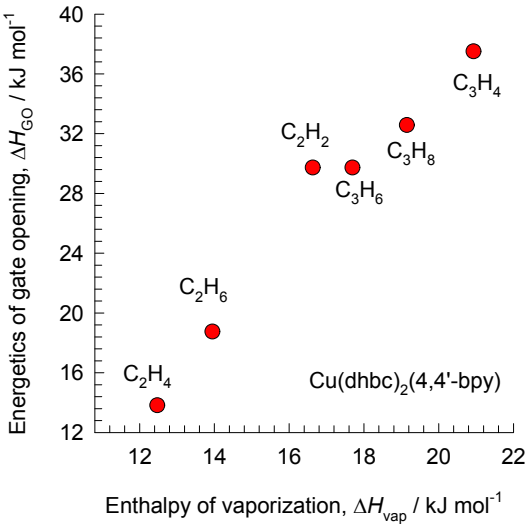

Figure S2. The molar enthalpy of gate opening, ΔH_{GO}, of C_2H_2, C_2H_4, C_2H_6, C_3H_4, C_3H_6, and C_3H_8 at 273 K, and 298 K in [Cu(dhbc)$_2$(4,4′-bipy)] plotted as a function of latent heats of vaporization.

4. Isosteric heat of adsorption

The isosteric heat of adsorption, Q_{st}, defined as

$$Q_{st} = RT^2\left(\frac{\partial \ln p}{\partial T}\right)_q \tag{6}$$

were determined using the pure component isotherm fits using the Clausius-Clapeyron equation.

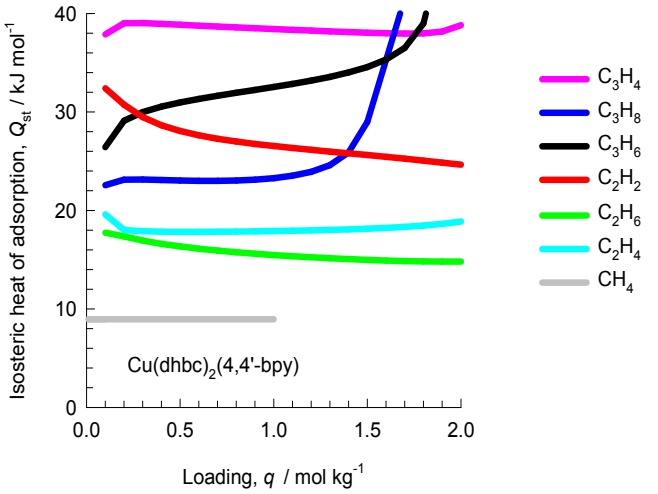

Figure S3. Comparison of the isosteric heat of adsorption of C1-C3 hydrocarbons in [Cu(dhbc)$_2$(4,4'-bipy)].

5. Grand canonical Monte Carlo (GCMC) simulations

Force fields and Simulation details

The potential parameters and partial charges for all of the adsorbates are shown in Table 6. C_2H_6 and C_2H_4 were modeled as a linear molecule with two charged LJ interaction sites, with C−C bond length l = 1.54 Å and 1.33 Å, respectively, taken from the EPM2 force field developed by Harris and Yung.[1]

Table 6 LJ potential and coulombic potential parameters for the adsorbates.

Adsorbate	Site	LJ parameters		
		σ(Å)	ε/k$_b$ (K)	charge (e)
C_2H_6	C_C	3.76	108.0	0.0
C_2H_4	C_C	3.96	56.0	0.0

The MOF material studied here was modeled by the atomistic representation. The LJ potential parameters for the framework atoms of the MOFs were taken from the Dreiding force field,[2] and

the missing parameters for Cu were taken from the universal force field (UFF),[3] as given in Table 7. The Lorentz–Berthelot mixing rules were used to determine all of the LJ cross-potential parameters of adsorbate–adsorbate and adsorbate–MOF interactions. In this work, atomic partial charges for the frameworks of the MOFs were estimated using the CBAC method developed by Zhong's group, with slight variation to make the total charge equal to zero.[4,5]

Table 7 LJ Potential Parameters for the Atoms in the Framework.

LJ parameters	Cu[a]	C	O	H	N
σ(Å)	3.11	3.47	3.03	2.85	3.26
ε/k_b (K)	2.516	47.86	48.16	7.65	38.95

[a] Taken from the UFF force field (it is missed in the Dreiding force field).

References

1. J. J. Potoff, J. I. Siepmann, AICHE J. **2001**, 47, 1676-1682.
2. S. L. Mayo, B. D. Olafson, W. A. Goddard, *J. Phys. Chem.* **1990**, 94, 8897-8909.
3. A. K. Rappe, C. J. Casewit, K. S. Colwell, W. A. Goddard, W. M. Skiff, *J. Am. Chem. Soc.* **1992**, 114, 10024-10035.
4. Q. Xu, C. Zhong, *J. Phys. Chem.* C. **2010**, 114, 5035-5042.
5. C. Zheng, C. Zhong, *J. Phys. Chem.* C. **2010**, 114, 9945-9951.

6. MD (Molecule Dynamic) simulations

MD simulations in the *NVT*-ensemble were performed to show gas separation behavior of the membranes by the Forcite module on the basis of the force field of condensed-phase optimized molecular potential for atomistic simulation studies (COMPASS).[1] The temperature was maintained at 273 K using the Andersen thermostat method. A combination of site–site Lennard-Jones (LJ) and Coulombic potentials was employed to determine the intermolecular interactions between adsorbates and adsorbates, as well as between adsorbates and MOF structures.[2-4] During the simulations, the MOFs structure was kept rigid, and C_2H_6 molecules were uniform distributed in the channels constitute an equilibrium system (Fig. 1A). Before MD simulations, the C_2H_6 molecules in one channel were labeled purple and first molecule was labeled yellow as shown in Figure 1 B and C.

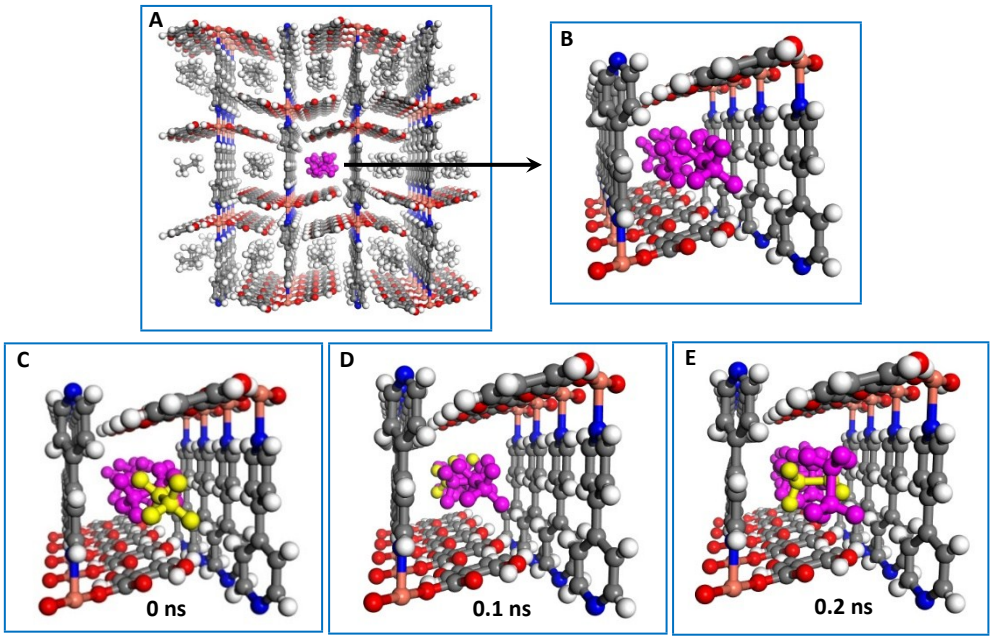

Figure S4. MD simulation for C_2H_6 molecules diffusion in the channels of [Cu(dhbc)$_2$(4,4'-bipy)] at 1 bar and 273 K.

After the MD simulation time of 0.2 ns, we can see that the labeled C_2H_6 molecular (yellow) can distributed randomly during the entire simulation. It indicated that C_2H_6 molecules can easily diffusion through the one-dimensional channels, and no pore size limitation to diffusion were found.

References

1. Q. Zheng, Y. Geng, S. Wang, Z. Li and J.-K. Kim, *Carbon*, **2010**, 48, 4315.
2. T. Wu, Q. Xue, C. Ling, M. Shan, Z. Liu, Y. Tao and X. Li, *J. Phys. Chem. C*, 2014, **118**, 7369.
3. Y. Tao, Q. Xue, Z. Liu, M. Shan, C. Ling, T. Wu and X. Li, *Acs Appl. Mater. Interfaces*, 2014, **6**, 8048.
4. M. Shan, Q. Xue, N. Jing, C. Ling, T. Zhang, Z. Yan and J. Zheng, *Nanoscale*, 2012, **4**, 5477.

7. IAST calculations of mixture adsorption

Briefly, the basic equation of the Ideal Adsorbed Solution Theory (IAST) theory of Myers and Prausnitz is the analogue of Raoult's law for vapor-liquid equilibrium, i.e.

$$f_i = P_i^0 x_i; \quad i = 1,2,...n \tag{7}$$

where x_i is the mole fraction in the adsorbed phase

$$x_i = \frac{q_i}{q_1 + q_2 + ...q_n} \tag{8}$$

and P_i^0 is the pressure for sorption of every component *i*, which yields the same spreading pressure, π for each of the pure components, as that for the mixture:

$$\frac{\pi A}{RT} = \int_0^{P_1^0} \frac{q_1^0(f)}{f} df = \int_0^{P_2^0} \frac{q_2^0(f)}{f} df = \int_0^{P_3^0} \frac{q_3^0(f)}{f} df = ... \tag{9}$$

where R is the gas constant (= 8.314 J mol^{-1} K^{-1}), and $q_i^0(f)$ is the *pure* component adsorption isotherm given by the Langmuir-Freundlich fits. The molar loadings $q_i^0(f)$ are expressed in the units of moles adsorbed per kg of framework, i.e. mol kg^{-1}. The units of the spreading pressure π is the same as that for surface tension, i.e. N m^{-1}.The quantity A on the left side of Equation (9) is the surface area per kg of framework, with units of m^2 kg^{-1}.

Each of the integrals in Equation (9) can be evaluated analytically. For the 3-site Langmuir-Freundlich isotherm, the integration yields

$$\int_{f=0}^{P} \frac{q^0(f)}{f} df = \frac{q_{A,sat}}{\nu_A} \ln\left(1 + b_A P^{\nu_A}\right) + \frac{q_{B,sat}}{\nu_B} \ln\left(1 + b_B P^{\nu_B}\right) + \frac{q_{c,sat}}{\nu_C} \ln\left(1 + b_C P^{\nu_C}\right) \tag{10}$$

The right hand side of equation (10) is a function of P. For multicomponent mixture adsorption, each of the equalities on the right hand side of Equation (9) must satisfied. These constraints may be solved using a suitable root-finder, to yield the set of values of P_1^0, P_2^0, P_3^0,.. P_n^0, all of which satisfy Equation (9). The corresponding values of the integrals using these as upper limits of integration must yield the same value of $\frac{\pi A}{RT}$ for each component; this ensures that the obtained solution is the correct one.

The adsorbed phase mole fractions x_i are then determined from

$$x_i = \frac{f_i}{P_i^0}; \quad i = 1,2,...n \tag{11}$$

The total amount adsorbed is calculated from

$$q_t \equiv q_1 + q_2 ... + q_n = \frac{1}{\frac{x_1}{q_1^0(P_1^0)} + \frac{x_2}{q_2^0(P_2^0)} + ... + \frac{x_n}{q_n^0(P_n^0)}} \tag{12}$$

The set of equations (7), (8), (9) (10), and (12) need to be solved numerically to obtain the loadings, q_i of the individual components in the mixture.

The selectivity of preferential adsorption of component i over component j can be defined as

$$S_{ads} = \frac{q_i / q_j}{p_i / p_j} \tag{13}$$

In equation (13), q_i and q_j are the *absolute* component loadings of the adsorbed phase in the mixture.

8. Transient breakthroughs in fixed bed adsorber

The performance of industrial fixed bed adsorbers is dictated by a combination of adsorption selectivity and uptake capacity. To demonstrate the selective adsorption of propyne using $Cu(dhbc)_2(4,4'\text{-bpy})$ we perform transient breakthrough simulations using the simulation methodology described in earlier work.

A brief summary of the breakthrough simulation methodology, essentially the same as that presente by Krishna, is provided below.

Assuming plug flow of an *n*-component gas mixture through a fixed bed maintained under isothermal conditions, the partial pressures in the gas phase at any position and instant of time are obtained by solving the following set of partial differential equations for each of the species *i* in the gas mixture.

$$\frac{1}{RT}\frac{\partial p_i(t,z)}{\partial t} = -\frac{1}{RT}\frac{\partial \left(v(t,z)p_i(t,z)\right)}{\partial z} - \frac{(1-\varepsilon)}{\varepsilon}\rho\frac{\partial \bar{q}_i(t,z)}{\partial t}; \quad i = 1,2,...n \tag{13}$$

In equation (13), t is the time, z is the distance along the adsorber, ρ is the framework density, ε is the bed voidage, v is the interstitial gas velocity, and $\bar{q}_i(t,z)$ is the *spatially averaged* molar loading within the crystallites of radius r_c, monitored at position z, and at time t.

At any time t, during the transient approach to thermodynamic equilibrium, the spatially averaged molar loading within the crystallite r_c is obtained by integration of the radial loading profile

$$\bar{q}_i(t) = \frac{3}{r_c^3}\int_0^{r_c} q_i(r,t)r^2 dr \tag{14}$$

For the breakthrough simulations presented in this article, we assume that intra-crystalline diffusion is of negligible importance. With this assumption the entire crystallite particle can be considered to be in thermodynamic equilibrium with the surrounding bulk gas phase at that time t,

and position z of the adsorber

$$\bar{q}_i(t,z) = q_i(t,z) \tag{15}$$

The molar loadings at any position z, at time t in Equation (15) are calculated on the basis of adsorption equilibrium with the bulk gas phase partial pressures p_i at that position z and time t. The adsorption equilibrium can be calculated on the basis of the Ideal Adsorbed Solution Theory (IAST) of Myers and Prausnitz. In all the simulation results we present in this article, the IAST calculations use Langmuir-Freundlich isotherm fits.

The *interstitial* gas velocity is related to the *superficial* gas velocity by

$$v = \frac{u}{\varepsilon} \tag{16}$$

In industrial practice, the most common operation is with to use a step-wise input of mixtures to be separation into an adsorber bed that is initially free of adsorbates, i.e. we have the initial condition

$$t = 0; \quad q_i(0,z) = 0 \tag{17}$$

At time, $t = 0$, the inlet to the adsorber, $z = 0$, is subjected to a step input of the n-component gas mixture and this step input is maintained till the end of the adsorption cycle when steady-state conditions are reached.

$$t \geq 0; \quad p_i(0,t) = p_{i0}; \quad u(0,t) = u \tag{18}$$

where u is the superficial gas velocity at the inlet to the adsorber. The model parameters are chosen on the basis of the experimental set-up and operating conditions.

9. Measurement of breakthrough experiment

The pelleting process of [Cu(dhbc)$_2$(4,4'-bipy)] particles were reported in our previous work.[1] In the separation experiment, [Cu(dhbc)$_2$(4,4'-bipy)] (4.1380 g) particles with diameters of 200-300 μm were prepared and packed into ϕ9×150 mm stainless steel column. The experimental set-up consisted of two fixed-bed stainless steel reactors. One reactor was loaded with the adsorbent, while the other reactor was used as a blank control group to stabilize the gas flow. The horizontal reactors were placed in a temperature controlled environment, maintained at 298 or 273 K. The

flow rates of all gases mixtures were regulated by mass flow controllers, an air cushion tank was placed to keep the gases mixtures well-mixed, and the effluent gas stream from the column is monitored by a gas chromatography. Prior to the breakthrough experiment, we activated the sample by flushing the adsorption bed with helium gas for 2 h at 373 K. Subsequently, the reactor was allowed to equilibrate at the measurement rate before we switched the gas flow.

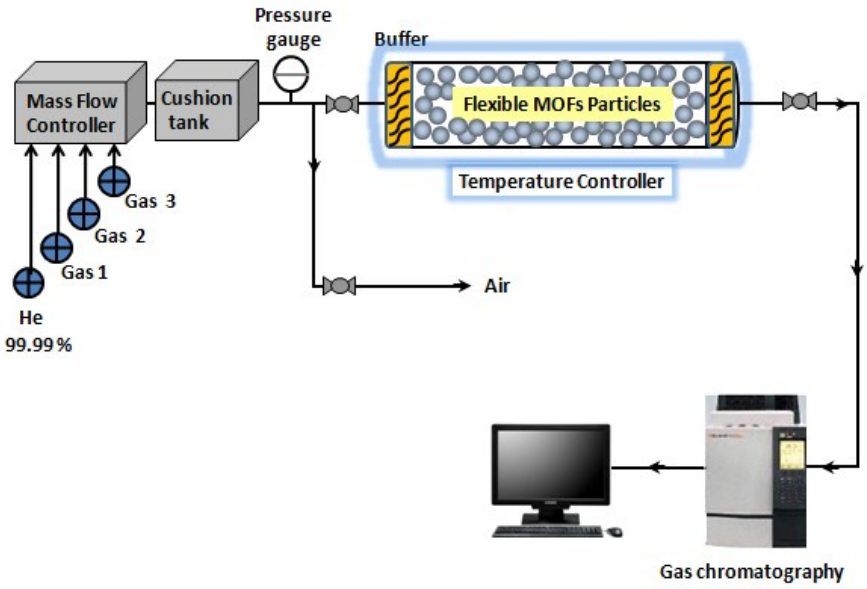

Figure S5. Breakthrough separation apparatus for flexible MOFs.

10. C_2H_2-C_2H_4-C_2H_6 separation

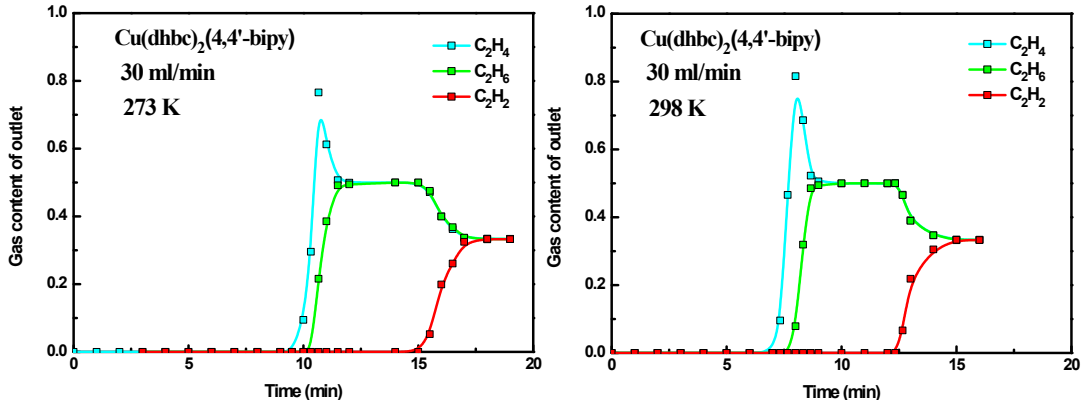

Figure S6. Breakthrough curves of [Cu(dhbc)$_2$(4,4'-bipy)] for separation equimolar 3-component C_2H_6-C_2H_4-C_2H_2 mixture in a fixed bed of adsorbent at flow rates of 30 ml/min at 1 bar and 273 and 298 K.

11. CH_4-C_2H_6-C_3H_8 separation

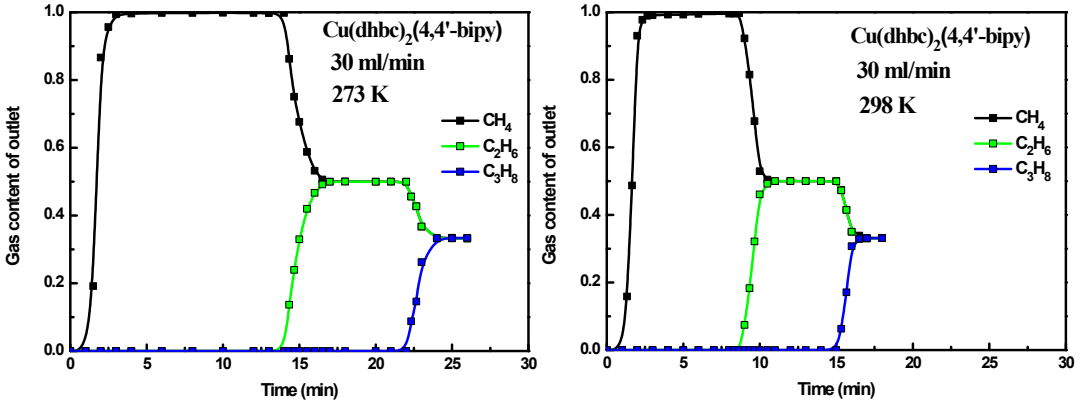

Figure S7. Breakthrough curves of [Cu(dhbc)$_2$(4,4'-bipy)] for separation equimolar 3-component CH_4-C_2H_6-C_3H_8 mixture in a fixed bed of adsorbent at flow rates of 30 ml/min at 1 bar and 273 and 298 K.

12. C_2H_4-C_3H_6 separation

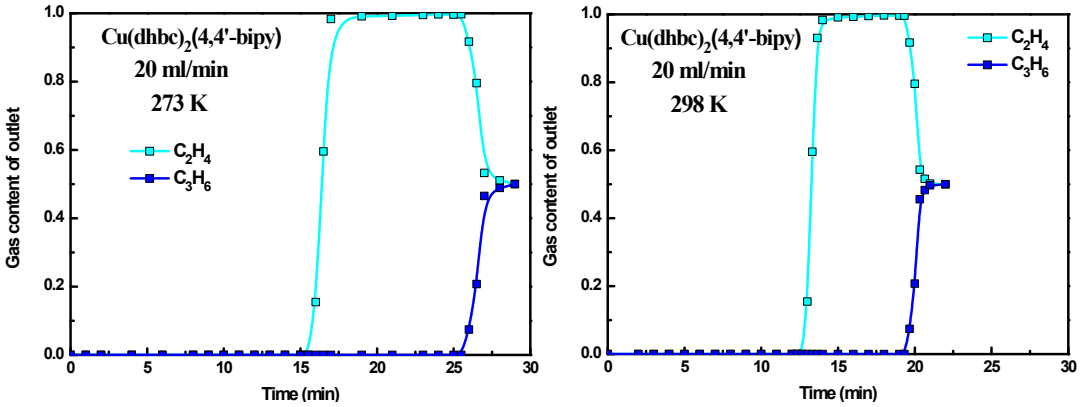

Figure S8. Breakthrough curves of [Cu(dhbc)$_2$(4,4'-bipy)] for separation equimolar C_2H_4-C_3H_6 mixture in a fixed bed of adsorbent at flow rates of 20 ml/min at 1 bar and 273 and 298 K.